Elsevier Editorial System(tm) for Corrosion Science
Manuscript Draft

Manuscript Number:

Title: Mechanical and electrochemical deterioration mechanisms in the tribocorrosion of Al alloys in NaCl and in $NaNO_3$ solutions

Article Type: Full Length Article

Keywords: A. Al-Si-Cu-Mg alloy; C. Tribocorrosion; C. Galvanic coupling

Corresponding Author: Mrs. Ana Catarina Vieira, M.D.

Corresponding Author's Institution: University of Minho

First Author: Ana Catarina Vieira, Master

Order of Authors: Ana Catarina Vieira, Master ; Ana Catarina Vieira, M.D.; Luís Augusto Rocha , Professor ; Nikolaos Papageorgiou, Senior researcher

Abstract: Tribocorrosion of Al-Si-Cu-Mg alloys was investigated in 0.05 M NaCl and 0.1 M $NaNO_3$ solutions under severe sliding and controlled electrochemical conditions. A simple galvanic coupling model was developed to analyze and quantitatively predict the evolution potential of the open circuit potential during tribocorrosion. According to this model and the obtained results, galvanic coupling was established in the $NaNO_3$ solution within the wear track between passive and mechanically depassivated areas. In the NaCl solution, galvanic coupling was established between the whole depassivated wear track and the surrounding area. This difference was attributed to different mechanical properties of the passive surfaces.

Lausanne, 26th January 2011

Dear Editor,

This manuscript deals with the tribocorrosion behaviour of Al-Cu-Mg-Si alloys in NaCl and $NaNO_3$ electrochemical solutions. The mechanical and electrochemical deterioration mechanisms of these materials were investigated under severe sliding and controlled electrochemical conditions. Although the wear-corrosion behaviour has been investigated in the past, the available information was focused on the wear behaviour of Al alloys. Therefore, one new aspect of this manuscript is the analysis of electrochemical response of aluminium under rubbing. Other novel aspect of this manuscript is the development of a galvanic coupling model to analyze and quantitatively predict the evolution potential of the open circuit potential during tribocorrosion. According to this model different galvanic coupling modes were established depending on the test solution. In the $NaNO_3$ solution, galvanic coupling was established within the wear track, between passive and mechanically depassivated areas while in the NaCl solution, galvanic coupling was established between the whole depassivated wear track and the surrounding area.

We think that this work provides new valuable insights into the wear-corrosion behaviour of the Al-alloys, as well as new valuable insights into the tribocorrosion field. These results are original, developed in our laboratories and are not submitted for publication elsewhere.

We hope this paper can be considered for publication in Corrosion Science.

Yours sincerely,

Ana Catarina Vieira

(corresponding author)

Ana Catarina Vieira (catarina.vieira@engmateriais.eng.uminho.pt)
PhD Student / Researcher
Centre for Mechanics and Materials Technologies (www.ct2m.uminho.pt)
Mechanical Engineering Department (DEM) - University of Minho
Campus de Azurem, 4800-058 Guimarães
Portugal
Tel: +351 253 510 220 / Fax: +351 253 516 007

Research highlights

1- First tribocorrosion investigation of Al alloys using electrochemical techniques.
2- First quantitative galvanic coupling model (depassivated vs. passive areas) predicting potential evolution during tribocorrosion.
3- Different galvanic coupling modes established in $NaNO_3$ and NaCl solutions.

Mechanical and electrochemical deterioration mechanisms in the tribocorrosion of Al alloys in NaCl and in $NaNO_3$ solutions

A.C. Vieira*

University of Minho, Centre for Mechanics and Materials Technologies (CT2M), 4800-058 Guimarães, Portugal;

catarina.vieira@engmateriais.eng.uminho.pt

L.A. Rocha

University of Minho, Centre for Mechanics and Materials Technologies (CT2M), 4800-058 Guimarães, Portugal;

lrocha@dem.uminho.pt

N. Papageorgiou

Ecole Polytechnique Fédérale de Lausanne (EPFL), Tribology and Interface Chemistry Group, 1015 Lausanne, Switzerland;

nikolaos.papageorgiou@epfl.ch

S. Mischler

Ecole Polytechnique Fédérale de Lausanne (EPFL), Tribology and Interface Chemistry Group, 1015 Lausanne, Switzerland;

stefano.mischler@epfl.ch

Abstract

Tribocorrosion of Al-Si-Cu-Mg alloys was investigated in 0.05 M NaCl and 0.1 M $NaNO_3$ solutions under severe sliding and controlled electrochemical conditions. A simple galvanic coupling model was developed to analyze and quantitatively predict the evolution potential of the open circuit potential during tribocorrosion. According to this model and the obtained results, galvanic coupling was established in the $NaNO_3$ solution within the wear track between passive and mechanically depassivated areas. In the NaCl solution, galvanic coupling was established between the whole depassivated wear track and the surrounding area. This difference was attributed to different mechanical properties of the passive surfaces.

Keywords: A. Al-Si-Cu-Mg alloy; C. Tribocorrosion; C. Galvanic coupling

*Correspondig author. Tel.: +351 253 510 220; fax: +351 253 516 007.
E-mail address: catarina.vieira@engmateriais.eng.uminho.pt (Ana Catarina Vieira)

1. Introduction

Aluminium alloys are attractive materials for many engineering applications (aerospace, transportation, watch and defence industries) essentially because these alloys generally presents low density combined with good mechanical properties and good corrosion resistance [1-3] provided by the thin passive films that spontaneously forms on aluminium in most of the neutral pH aqueous solutions.

In many applications, such as bearings and engine blocks [4], aluminium alloys may be subject to tribological conditions leading to wear. In this case it is essential to increase the wear resistance by using appropriate alloying and heat treatments [1,5-7] or by introducing reinforcing hard phases such as Si [3,8] and/or SiC [7,9,10]. When a contact operates in a corrosive environment its deterioration can be significantly affected by surface chemical phenomena. For example under sliding [11-13] or erosive conditions [12] passive film can be removed by abrasion thus exposing the underlying reactive material to more severe corrosion. On the other hand surface films were found modifying the mechanical behaviour of the underlying metal and thus its wear response [14]. This type of corrosion-wear interactions is known as tribocorrosion, i.e. a form of surface alteration involving the joint action of a moving contact and chemical reactions in which the result may be different in effect than either process acting separately [15]. Results from the literature indicate the occurrence of wear-corrosion interactions in the tribocorrosion of aluminium alloys. H. Mindivan et al [6] studied the wear behaviour of 7039 Al alloy (Al-Zn alloy) under dry (reciprocating wear tests using 1.5N as normal applied load and a 10mm diameter Al_2O_3 ball as counterbody) and in corrosive wear (same tribological conditions as used in dry tests plus a 3 g/l NCL + 10 ml/l HCl solution) conditions. The authors compared two heat-treated alloys: a T6 (age-hardened) alloy and a RRA ("retrogression and re-aging") treated alloy. Although the dry sliding wear resistance of the RRA treated alloy (higher hardness and strength) was higher than the T6 treated alloy, in tribocorrosion the behaviour of this material was the worst. C.N. Panagopoulos et al [16] studied the corrosive wear of 6082 aluminium alloy (Al-Si-Mg alloy) rubbing against a stainless steel counterbody in 0.01M NaCl solution. A pin-on-disk configuration was used (0.3m/s of sliding speed, 5N as applied load during 55.5min under free corrosion conditions). Al alloys failed mainly by plastic deformation, abrasion and cracking. W.B. Bouaeshi et al [7] added Y_2O_3 to aluminium in order to strengthen the material without decreasing the corrosion resistance. The wear behaviour was evaluated in a pin-on-disk tribometer, using a Si_3N_4 sphere as

counterbody. The tests were done using different normal loads, sliding speed of 2 cm/s and using two different electrochemical solutions: 0.1M H_2SO_4 and 3.5% NaCl. The volume loss increased with the increase of the applied normal load. The finer microstructure obtained after yttria addition, resulted in higher resistance to tribocorrosion.

Despite this evidence for wear-corrosion interactions during tribocorrosion of aluminium alloys, the involved mechanisms remain largely unknown. Some authors reported that tribocorrosion of Al alloys (in NaCl based solutions) was characterised by adhesive wear, abrasive wear and plastic deformation [6-8]. However, no information about the corrosion behaviour of aluminium under tribological conditions was reported. In the case of passive aluminium one would expect a significant increase in corrosion rate due to the mechanical removal of the passive film and the exposure of bare metal to the solution. This work was initiated with the aim to gain a better insight into the wear and electrochemical response of aluminium alloys subject to tribocorrosion in aqueous solutions. For this the tribocorrosion of model age-hardened Al-10Si-4.5Cu-2Mg cast alloys was investigated using a laboratory tribometer equipped with an electrochemical cell. The effect of solution composition (0.05M NaCl and 0.1M $NaNO_3$), electrode potentials and the applied normal loads (4N and 1.3N) was considered. Nitrate solutions are known to promote passivity of aluminium alloys while chloride ions are known to weaken passivity and to promote local depassivation and pitting corrosion.

Two typical triboelectrochemical experiments [11] were conducted: open circuit potential measurements and potentiostatic tests. The latter technique consists in imposing a well-defined potential to the tested metal using a potentiostat. At the onset of rubbing an increase of the anodic current, and thus of the metal oxidation rate, is usually observed due to the periodical removal of the film followed by the enhanced corrosion (wear accelerated corrosion) until the film forms again. The amount of wear accelerated corrosion can be easily quantified, provided metal oxidation is the only reaction affected by rubbing, by integrating the excess current and converting it into removed metal volume by using Faraday's law [11]. The potentiostatic technique is well suited for fundamental investigations and has lead to the development mechanistic models of wear accelerated corrosion [17] that describes the effect of normal load, metal hardness, sliding velocity and passivation charge.

However, in typical engineering situations the electrode potential is not imposed through an external potentiostatic circuit and can thus vary with time depending on the

variability of the experimental conditions. The electrode potential spontaneously establishing between metal and solution is thus called “open circuit potential” (OCP). Rubbing may shift significantly OCP values because a galvanic coupling establishes between the depassivated worn area and the surrounding passive surface. Since the electrode potential drives the electrochemical reactions, its evolution in the course of rubbing is a critical factor affecting metal oxidation and overall degradation. The variation of OCP during an experiment can be easily followed by using an appropriate reference electrode connected to the investigated metal through a voltmeter. However, up to date no theoretical models are available for its quantitative interpretation and thus the useful information extractable from OCP measurements is at present rather limited despite the practical relevance for tribocorrosion of engineering systems. For this reason a simple galvanic coupling model commonly used in corrosion [18] was adapted to the tribocorrosion situation in order to mechanistically interpret the evolution of OCP during rubbing.

2. A galvanic cell model for tribocorrosion at open circuit potential

The cathodic shift of potential usually observed during tribocorrosion of passive metals is explained by the galvanic coupling established between the mechanically depassivated areas (anode) and the surrounding passive areas (cathode) [19]. The depassivated areas act as anode where metal oxidation is the dominating electrochemical reaction. Anodic oxidation leads to metal dissolution and, if the time interval between two successive passes is high enough, to the re-growth of the passive film. In neutral solutions, the reduction of water and/or oxygen is the dominating cathodic reaction. A galvanic ionic current flow from the anode through the solution to the cathode where electrons liberated at the anode by the metal oxidation and flowing through the metal are consumed by the reduction reaction. Note that reduction of water and oxygen occurs in principle also on the anodes: however, this contribution is neglected here because in the present experiments (see section 4) the worn area is much smaller than the electrode surface area.

In a galvanic cell the anodic current I_a is equal to the absolute cathodic current I_c (as convention, cathodic currents are negative while anodic are positive). Considering the cathodic i_c and anodic i_a current densities (current per unit area), one can write for the case of tribocorrosion experiments:

1) $I_a = - I_c <=> i_a A_a = - i_c A_c$

where A_a and A_c correspond to the surface areas of the anode and of the cathode, respectively. Here it is assumed that the current density is homogenous over the cathodic and anodic sites. In reality, local variations in galvanic current can be expected due to the deformed state of the rubbed metal. Indeed, H. Krawiec et al [20] observed, using SRET, heterogeneities in anodic current distribution within wear tracks formed on stainless steel.

The difference between cathode potential E_c and anode potential E_a corresponds to the ohmic drop ($R_{ohm} I_a$) occurring in the solution (the relatively small electronic resistance of the metal is neglected) according to:

2) $E_a = E_c – R_{ohm} I_a$

where R_{ohm} is the ionic resistance of the solution located between cathode and anode. The relation between cathode potential E_c and the current density i_c can be determined empirically by a Tafel interpolation of the linear part of the cathodic branch of the polarisation curve. This yields equation 3:

3) $E_c = E_{corr} + a_c – b_c \log |i_c|$

where a_c and b_c are constants and E_{corr} the corrosion potential of the passivated metal (i.e. the potential at which the current changes sign in the polarisation curves). Combining equations 1 and 3 yields:

4) $E_c = E_{corr} + a_c – b_c \log (i_a A_a/A_c) = E_{corr} + a_c – b_c \log i_a – b_c \log (A_a/A_c)$

According to equation 4, the cathode potential in the galvanic coupling depends mainly on two factors: the anodic current and the anode to cathode area ratio. The anodic current is, due to the cyclic depassivation/repassivation process, established in the rubbed area. Between two strokes the passive film growths in the depassivated areas up to a certain thickness depending on the stroke frequency, electrode potential and passivation kinetics. The film re-growth requires a certain anodic charge density

(passivation charge density q_p in C/m^2). Accordingly, the current density i_a is given by equation 5 where f is the stroke frequency (Hz):

5) $i_a = q_p (E_a) f$

Equation 5 implies that the current i_a does not change in the course of an experiment at constant potential. In the case of OCP tribocorrosion tests q_p is expected to change to some extent during the initial potential drop but to remain nearly constant once a steady state potential is reached during tribocorrosion.

In tribocorrosion, two limiting galvanic coupling situations can theoretically arise (Figure 1): galvanic coupling between the completely depassivated wear track and the area surrounding it (Figure 1a) or galvanic coupling between depassivated and still passive areas within the wear track (Figure 1b). Films that are mechanically weak and easy to remove should promote the former situation while adherent, thick and resistant passive films lead to the latter. High loads should also favour the complete depassivation of the wear track. In real cases both limiting situations are likely combined and galvanic coupling occurs between depassivated area and passive areas within and outside the wear track.

The evolution of the A_a/A_c ratio during rubbing depends on the coupling situation. In the case of galvanic coupling within the wear track (Figure 1b) this ratio depends on the percentage of depassivated area inside the wear scar. This percentage is not expected to change during an experiment and does not depend significantly on normal force as long as the contact pressure remains high enough to provoke large plastic deformation and depassivation. In case of the galvanic coupling illustrated in Figure 1a) (between wear track and surrounding area) the A_a/A_c ratio increases significantly with the progress of wear and the corresponding enlargement of the wear track. Further, this ratio is expected to increases proportionally to the applied load as wear becomes more severe. This simple model allows one to relate the evolution of the electrode potential during a tribocorrosion test with the extent of wear and thus to mechanical and material properties. Further, the influence of the cathodic current kinetics or cathode kinetics can also be assessed.

3. Materials and Methods

3.1 Materials

A non-commercial Al-10Si-4.5Cu-2Mg (wt.%) alloy was home-developed in order to present specific properties. Si was added to improve the castability properties and Cu and Mg were considered to improve the mechanical properties of the alloy by age-hardening heat-treatment. The alloy was fabricated by centrifugal casting (radial geometry with 1500 rpm as centrifugal speed). After, age-hardening heat treatments were performed. The solution heat-treatment was done in a tubular furnace 500 °C, either during 2h or 8h. This treatment was followed by water quenching and artificial aging at 160 °C during 512 min (thermostatic silicone bath). In this paper, the samples solution treated during 2h are identified as *Al-S2h* while the samples solution treated during 8h are identified as *Al-S8h*. To be used as reference, a non heat-treated sample was also studied and is identified as *Al-NHT*.

The microstructure of the Al-10Si-4.5Cu-2Mg (wt.%) alloy (without heat-treatment and after heat-treatment) as well as their constituent phases were characterized and described in detail elsewhere [21]. The constituent phases are α-Al, Si, θ-Al_2Cu, Q-$Al_4Cu_2Mg_8Si_7$ and π-$Al_8Si_6Mg_3Fe$. The hardness is HV_{30} = 109 ± 2, HV_{30} = 167 ± 6 and HV_{30} = 172 ± 5 in the Al-NHT, Al-S2h and Al-S8h samples, respectively. The yield strength expected with these thermal treatments is in the order of 0.4 GPa [22].

3.2 Corrosion tests

The samples were wet-polished up to 1200 mesh (SiC abrasive paper) previous to each corrosion test. Two electrochemical solutions were used: 0.05M NaCl (purity ≥ 99.5%, Merck) and 0.1M $NaNO_3$ (purity ≥ 99 %, Merck), presenting pH = 6.2 and pH = 6.8, respectively. The pH was measured before and after the corrosion tests and no variation was detected. The tests were made at controlled temperature (25 °C) in aerated controlled conditions using a calomel reference electrode (SCE) placed in a Luggin capillary, Pt counter electrode (CE) and Al-NHT, Al-S2h and Al-S8h samples as working electrodes (WE). Polarization measurements using a potential sweep rate of 0.5mV/s in noble direction were performed (starting from cathodic values). The electrochemical measurements were carried out in Autolab PG Stat 30 Potentiostat / Galvanostat equipment under software GPES Manager to monitor and save the data.

3.3 Tribocorrosion tests

Disks were machined from the centrifugal cast Al alloys, with ∅ = 20 mm (+/- 0.1 mm) and 5 mm (+/- 0.1) thick. Previous to each tribocorrosion test, the samples were wet-grinded up to 4000 mesh (SiC abrasive paper) and polished up to 3 µm (diamond spray - Struers). The electrochemical solutions were the same described above and the disk surface area exposed to the electrolyte was 2.5 cm^2. The pH of the electrolyte was measured before and after the tests (at approximately 22 °C and relative humidity of 40%). No variation was detected. Tribocorrosion tests were performed using a reciprocating ball-on-plate tribometer (ball sliding against a stationary working electrode), 1Hz frequency, 4 mm stroke length and a 11.4 mm/s sliding velocity, 4N and 1.3N as normal applied load (corresponding to a maximum Hertzian pressure of 0.69 GPa and 0.47 GPa, respectively). The counterbody was an alumina ball (∅ = 6 mm). A new alumina ball was used in each test.

The reciprocating sliding tribometer used in the present study is described in more details elsewhere [23]. The friction coefficient and the relevant electrochemical parameters were continuously monitored by using LabView based software. A three electrodes electrochemical cell was mounted on the tribometer (Figure 2). The samples disks were connected to a Wenking LB 95 L potentiostat as working electrode. A Pt wire served as counter electrode and a commercial calomel reference electrode was placed at a distance of 20 mm from the wear track. All the potentials values in this paper are measured in relation to SCE.

The tests were done under three different potentials: at OCP, with cathodic applied potential (-0.8 V in NaCl, -0.6 V in $NaNO_3$) and with anodic applied potential (-0.4 V in NaCl, 0.2 V in $NaNO_3$). Stabilization at the selected potentials was done during 10 min, before rubbing. Then rubbing starts and this step duration was 10 min. After the end of rubbing, the samples were kept in the selected potential during 10 min.

The worn surfaces were analysed by SEM/EDS. EDS spectra were obtained under an acceleration voltage of 15 KeV. The SEM/EDS equipment used were a Nano-SEM model – FEI Nova 200 and a JEOL 6300 microscope.

The profiles of the wear tracks were quantified using non-contact scanning laser profilometry (UBM Telefokus instrument). Three profiles across the wear track for each sample were measured. The wear volume was calculated by multiplying the depth mean values by the track's length and by the width.

Micro-hardness was measured, inside and outside of the wear scar using a Leitz Weitzlar 721 300 device. The applied load used was 200g, during 15s. Five indentations were made in each case.

4. Results

4.1 Corrosion behaviour

The polarization curves of the different alloys obtained in the NaCl and in the $NaNO_3$ solutions are presented in Figure 3a) and in Figure 3b), respectively. Reproducibility in the NaCl solution (Figure 3a) was good. All the alloys behaved similarly with the anodic domain above the corrosion potential E_{corr} (≈ -0.60V) characterised by large current densities indicating an active type dissolution regime. The differences in the anodic current observed between the various samples were attributed to copper dissolution from the Cu-rich phases into the α-aluminium phase occurring during solution heat treatment [21]. The corrosion resistance of the α-aluminium phase is known to increase with Cu content [24].

The behaviour in $NaNO_3$ solution (Figure 3b) was quite different. First, relatively poor reproducibility in the corrosion potential values was observed. Indeed the E_{corr} values varied between approximately –0.5V to –0.2V irrespective of alloy type. The cathodic current was reproducible and clearly decreases for the alloys underwent aging. Passive currents varied between 0.01 and 0.1 mA/cm^2 irrespective of the alloy.

4.2 Friction and wear behaviour

The average friction coefficient values plotted in Figure 4 were calculated by averaging over the entire rubbing duration the instantaneous value measured during the tests. The values lie between 0.4 and 0.5 and without any significant influence of potential or age-hardening. Only in NaCl, age-hardening seems to promote a slight decrease in friction. Tests carried out under a load of 1.3 N exhibit similar values of the coefficient of friction as measured at higher load.

Wear scars of typical width ranging between 0.3 to 0.7 mm, depending on test conditions, were formed on the aluminium samples. The volumes of the wear scars are presented in Figure 5 for the different alloys, potential, loads and solutions. Significantly less wear is observed at lower loads. Age-hardened alloys (Al-S2h and Al-

S8h) exhibit lower wear compared to the untreated alloy in all solutions and at all potentials. This is probably related to their higher hardness. The potential has little influence on the wear volume in the NaCl solution.

In the $NaNO_3$ solution, less wear is observed at OCP while similar wear volumes are found at cathodic and anodic potentials.

The effect of solution depends on potential and alloy. While the Al-S8h samples exhibit less wear in the $NaNO_3$ solution at all potentials the solution composition does not affect the wear rate of Al-S2h samples. At OCP the untreated alloy suffer of less wear in the $NaNO_3$ solution compared to the NaCl solution while no significant solution effect can be observed at imposed cathodic or anodic potential.

Regarding load effect, with lower load, lower wear volume values were reached, being however the hardness effect present, this is, higher wear volume in Al-NHT.

All wear scars exhibited similar wear patterns as illustrated by the SEM images in Figure 6. Worn surfaces show large plastic flow with ridge formation. Wear particles are apparently formed by breakdown of the ridge sides. Such large plastic flow is not surprisingly since the maximum contact pressure here exceeds the yield strength of the soft aluminium alloys and thus surface and subsurface plastic shear occurs [19,25]. This large plastic flow results in work hardening as confirmed by the micro-hardness values listed in Table 1. According to the difference in micro-hardness values obtained inside and outside of the wear track after the tribocorrosion tests (Table 1), the extent of hardening is similar for all alloys and solutions. In Table 1 only values obtained in OCP conditions using 4N as normal applied load were presented. However, similar hardness values were found under applied cathodic or anodic potential as well as with lower load (1.3N).

Plastic flow resulted in transfer of aluminium alloy to the alumina counter ball as shown in the SEM micrograph shown in Figure 7.

4.3. Electrochemical response to sliding

Figure 8 shows the evolution the OCP during wear tests for different alloys and loads. After rubbing starts (at approximately 600s) the OCP shifts progressively to lower values when compared to the initial potential (-0.6 V in NaCl - Figure 8a, -0.2 V in $NaNO_3$ - Figure 8c). This fact is normally attributed to passive film destruction by the abrading action of the counter piece. Subsequently, more reactive bare metal is exposed

to the solution [11,26]. After rubbing stops, the OCP recovers the initial value established before rubbing. The evolution of OCP depends on the solution. In the $NaNO_3$ solution (Figure 8c), the OCP shift occurs more rapidly at the onset of rubbing and a steady state value is reached after less than 100s. Further, the load does not affect the OCP drift in $NaNO_3$ (Figure 8d) while in NaCl (Figure 8b) the OCP drop is significantly smaller at lower load.

The evolution of current during testing at imposed cathodic potential is shown in Figure 9a) and Figure 9b), obtained in NaCl and in $NaNO_3$ solutions, respectively. In static conditions the current at cathodic potentials is negative because of the dominating reduction reaction of water and nitrates. Interestingly, rubbing reduces the amplitude of the cathodic current and this for all solutions and alloys. In the case of the alloys tested in NaCl solution (Figure 9a), the current attains even positive values indicating that the oxidation current becomes larger in the curse of the experiment than the reduction current. This suggests that rubbing accelerates the anodic oxidation of aluminium, a reaction that is thermodynamically possible for all potentials above the reversible potential of aluminium, which value is approximately –1.9 V vs. SCE according to the Pourbaix diagrams [27]. At the end of rubbing, mechanical activation ceases and the current recovers the initial value.

The electrochemical response at imposed anodic potential depends on the solution (Figure 10). In the NaCl solution (Figure 10a) rubbing does not affect significantly the current and this independently on heat treatment. This behaviour was already reported [28] for the case of active metals, i.e. metal dissolving in absence of passive film. In the $NaNO_3$ solution (Figure 10b) the potential lies in the passive domain. The current suddenly increases at the onset of rubbing because of mechanical breakdown of the passive film [11]. This current enhancement is largest in the case of the non age-hardened alloy (Al-NHT) and lowest for the Al-S8h alloy. At the end of rubbing the current of the Al-S2h and Al-S8h samples decreases rapidly to the value observed before rubbing while the current drop is much slower in the case of Al-NHT. This indicates that age hardening promotes the capability of the alloy to repassivate after mechanical activation.

5. Discussion

5.1 Material degradation mechanisms

The SEM pictures (Figure 6 and 7) clearly indicate that the aluminium surface underwent large plastic flow during rubbing for all the tested conditions. This situation of grooving wear [29] is characteristic of highly loaded contacts between hard counter body (alumina in this case) and softer materials (aluminium alloy here) and may imply different wear mechanisms such as adhesion, abrasion and fatigue. Indeed, the transference of aluminium to the alumina counter body surface (Figure 7) indicates that adhesive wear occurs. Smearing and detachment of material on the edge sides of asperities sliding on aluminium is another wear mechanism (Figure 6) related to abrasion. Fatigue wear manifest itself by subsurface cracks that, when emerging to the surface, lead to particle detachment. However, no cracks are visible in the SEM (Figure 6) images and therefore fatigue seems not to play a major role here.

The increase in anodic current observed during rubbing in Figure 9 and Figure 10 indicates that wear accelerated corrosion from depassivated areas contributes to the overall material deterioration. Wear accelerated corrosion is a chemical removal mechanism (chemical wear) distinct from the mechanical wear mechanisms listed above (adhesion, abrasion). According to [13], the total wear volume W_T corresponds to the sum of the individual contribution of the mechanical wear V_{mec} and the chemical wear V_{chem}. In tribocorrosion tests carried out under applied anodic potential the chemical wear can be calculated from Faraday's law according to:

6) $V_{chem} = Q\, M / n\, F\, \rho$

where Q is the excess anodic electrical charge (C) due to wear accelerated corrosion, M is the atomic mass of the metal, n is the charge number for the oxidation reaction, F is the Faraday constant (C/mol) and ρ is the density of the metal (g/cm^3). The excess charge can be determined by integrating the excess current, this is, the difference between average current during rubbing and current just before the onset of rubbing, over the sliding duration. This calculation is valid only if the anodic oxidation of the metal is the only significant electrochemical reaction contributing to the excess current. Thus equation 6 can be applied in the present case to the tests carried out at anodic potential but not at the cathodic one, where changes in the cathodic reactions can also

influence the excess current (Figure 10b). Considering n=3 and ρ = 2.7 g/cm^3, the calculated contribution of mechanical wear and the chemical wear are presented in Figure 11. These results indicate a small contribution of wear accelerated corrosion (responsible for chemical wear) to the overall wear that is mainly determined by mechanical degradation.

5.2 Electrochemical mechanisms: applied potential

The nature of the solution significantly affects the electrochemical response of the investigated alloy with rubbing. The differences found at anodic potential (Figure 10) can easily be related to the different surface chemical state found in the two solutions: passive state in $NaNO_3$ and active state in the NaCl solution. In the $NaNO_3$ solution rubbing removes the passive film and enhanced anodic metal oxidation takes place in the exposed bare metal until the passive film forms again. Indeed, as rubbing stops the current decreases again towards the initial value. The fact that the decrease is slower in case of the un-treated alloy, suggest that passivation occurs faster on age hardened alloys.

At cathodic potential, aluminium is expected to be passive despite the dominating cathodic reduction reaction. In the present solutions, aluminium can thermodynamically oxidise to $Al(OH)_3$ for all potentials above its reversible potential, which is approximately –1.9 V vs. SCE according to [18,27]. If $Al(OH)_3$ forms, it can act as a passive film, thus limiting the reaction rate (passivity).

5.3 Electrochemical mechanisms: open circuit potential

Differences between solutions are more marked at open circuit potential (Figure 8). In both solutions the potential shifts negatively during rubbing. However, in tests carried out in $NaNO_3$ solution, rubbing manifests itself by a sharp cathodic shift of the potential, which attains quickly a steady state value (Figure 8c). Moreover, the shift amplitude is independent on load (Figure 8d) and thus on wear scar size. This behaviour is consistent with the electrochemical model postulated in Figure 1b) involving galvanic coupling within the wear track.

In NaCl solutions the behaviour is different. Indeed a continuous decrease in potential is observed during rubbing (Figure 8a) instead of the sharp drop observed in $NaNO_3$ solutions (Figure 8c). Further extent of cathodic shift is less pronounced at lower loads where wear is less severe. The electrochemical behaviour during tribocorrosion in NaCl

is compatible with the galvanic coupling model depicted in Figure 1a) between the wear track and the surrounding passive area.

The different behaviour in the two solutions may be related to the different nature of the passive film which composition and thickness can be largely affected by the anions present in the electrolytes. Indeed chloride ions are known to thin the passive films and to weaken it by substituting oxygen ions in the oxide lattice. Indeed, while a wide passive domain is observed in the polarisation curves measured $NaNO_3$ (Figure 3b), the anodic behaviour in the NaCl solution is characterised already above –0.6 V by an active like dissolution resulting in large currents (Figure 3a).

5.4 Quantitative prediction of potential drop in case of galvanic coupling between wear track and surrounding area

For the situation illustrated in Figure 1a), equation 5 can be used to quantitatively evaluate the evolution of the open circuit potential during rubbing in NaCl by assuming that the wear track area A_{wt} corresponds to the anodic area A_a while the rest of the electrode surface constitutes the cathode which area is A_{owt} (area outside the wear track). As a consequence of wear A_{wt} increases with rubbing time.

The wear track area A_{wt} corresponds to the wear track length multiplied by the cord length of the circular segment and is given by equation 7):

7) $A_{wt} = L\ R\ \theta$

The wear track area A_{wt} can be extracted from the instantaneous wear track volume. The wear track volume V can be approximately calculated by multiplying the stroke length L by the area of the circular segment (A_{cs}) defined by the alumina ball (of radius R) impinging into the metal according to equation 8:

8) $V = L\ A_{cs} = L\ 0.5\ R^2\ (\theta\text{-}\sin\theta)$

where θ (rad) is the central angle defining the circular segment. For angles lower than 0.6 (i.e wear scar width lower than 1.75 mm), equation 7 can be empirically simplified with less than 1% error (considering L = 0.4 cm, R = 0.3 cm as described in the experimental section) by equation 9:

9) $V = 0.003\ \theta^3$

Additionally, according to Archard wear law, a linear relationship between the wear volume (V) and rubbing time (t) can be assumed:

10) $V(t) = C_w\ t$

where C_w is a constant that can be calculated by dividing the wear track volume measured at the end of the test by the rubbing duration. Extracting θ from equation 9 and considering equation 10 to define V, equation 7 can be rewritten as:

11) $A_{wt} = L\ R\ (C_w\ t / 0.003)^{0.333}$

Therefore, E_c can be defined as:

12) $E_c = E_{corr} + a_c - b_c \log i_a - b_c \log [(L\ R / A_{owt})\ (C_w\ t / 0.003)^{0.333}]$

where a_c and b_c are the parameters determined by interpolation of the cathodic branch of the polarisation curve, which clearly extends into high field Tafel regime. (Figure 3a). Their values have been determined experimentally to be –0.74V and 0.41V/decade, respectively.

In principle i_a and A_{owt} are a function of time. Due to the small size of the wear track compared to the overall electrode, we can reasonably assume that in the present case A_{owt} is constant with time and corresponds approximately to the electrode area. The anodic current density i_a corresponds to the passivation charge density passed at each stroke to repassivate the wear track. The passivation charge density may be affected by the electrode potential [30] and thus it may vary during a tribocorrosion experiment. However, no data are available on the evolution of passivation charge density and potential for aluminium. So, the i_a values must be arbitrarily chosen and therefore serve in this instance as the model parameter.

Figure 12 shows E_c values calculated using equation 12 with i_a values used as a fitting parameter. Also included in Figure 12 are the experimentally obtained results. The theoretical values fitted for i_a = 9.5 mA/cm^2 are in good agreement with the

experimental values. Considering the typical dimension of a wear scar (0.3 to 0.7 mm width and 4 mm in length) this current density corresponds to I_a values ranging from 0.1 to 0.3 mA, i.e. the same order of magnitude as the currents measured during rubbing (Figures 9 and 10). Considering that, the E_c values should be equal or higher than the measured values but lower than the open circuit potential established before rubbing, values of i_a much smaller (7.5 mA/cm^2) or much greater (13 mA/cm^2) than 9.5 mA/cm^2 yield unrealistic too high or too low potentials, respectively.

Figure 13 is a graphical representation of equation 12 and equation 2, considering time independent i_a values of 9.5 mA/cm^2. The C_w value was extracted from the average wear volume of Al-NHT worn samples in NaCl (Figure 5). Experimental points from two independent tribocorrosion tests of Al-NHT samples are also shown.
Pearson et al [31] proposed a simple formula (equation 13) to calculate the ohmic resistance of a rectangular strip electrode representing a scratch in a metal surface as a function of its dimensions.

$$13) \quad R_{ohm} = 1 / (2 \pi \kappa b) (\ln (2 b/a)+1)$$

with κ the solution conductivity (4.5 mS.cm) and a and b the semi-width and the semi-length of the strip electrode. This formula was found to reasonably well describe the ohmic resistance established in tribocorrosion wear tracks [32,33] despite the fact that it does not take into account the presence of the counter-body [33]. Previous work has shown that formula of equation 13 can underestimate the actual ohmic resistance by approx. 15% under the experimental conditions employed [34]. By considering that a = 0.5 A_{wt}/L and b is constant (2 mm, i.e. half stroke length) one can calculate at each time the value of R_{ohm} by using equation 11 and 13. The instantaneous E_a value plotted in Figure 13 were obtained using equation 2 and by taking I_a as the current, i.e. the density i_a (9.5 mA/cm^2) multiplied by A_{wt}. Of course, equation 13 applies in the case of a uniform current density within the track which could be a good approximation of the current distribution here as: 1) slight embedment of the electrode i.e. a recessed electrode geometry, will provide a finite current at the edges, while presenting minimal resistance, thus limiting the 'edge effect' 2) for the secondary distribution in the 'high field' Tafel regime, the combination of surface resistance associated with the limited reversibility of the electrode kinetics typically leads to more uniform current

distribution [35-38]. It is noteworthy that the E_a simulation values, calculated on the basis of the various resistance formulations, more or less rest in a narrow band, the only important difference resulting from the incorporation of the screening effect of the alumina sphere- ca. 50% higher than the predicted [17].

Figure 13 shows a reasonable good correlation between the model predictions and experimental data, with the experimental points lying on or in between the theoretical predictions for E_a and E_c and showing the same decreasing trend. This lends support to the simple galvanic coupling model illustrated in Figure 1a) and described by equation 4, especially when considering that the experimental error due to the IR-drop introduced during the measurement of E_c (potential between the reference and WE) is higher and therefore the deviation from experiment greater as the current increases. Moreover, the mixed potential of the anode E_a lies well above the aluminium reversible potential (approx. –1.9 V vs. SCE), by which threshold E_a should in any case be thermodynamically limited. However, the quantification approach taken here neglects relevant effects, i.e. the increase of the wear track area induced by surface roughening or debris particles formation, the deviation from the Archard wear behaviour in the initial run in wear regime and non homogeneous potential distribution on the sample surface. Further, only approximate values for R_{ohm} and i_a were used. Clearly, these aspects must be considered in order to develop a robust predictive model. Nevertheless, this preliminary attempt shows the feasibility and the appropriateness of the galvanic coupling model.

5. Conclusions

1. The overall degradation of the aluminium alloy was found to be mainly controlled by mechanical wear while wear accelerated corrosion little contributed. Age-hardened alloys exhibited less wear due to their increased hardness.
2. Wear rates in $NaNO_3$ solutions are slightly lower than in NaCl. Differences in electrochemical response appear between the solutions depending on prevailing electrochemical and loading conditions. At applied cathodic potentials rubbing resulted in an anodic current enhancement in both solutions indicating passive behaviour. At applied anodic potential Al dissolved actively in the NaCl solution and no noticeable effect of rubbing was observed. In $NaNO_3$, the considered Al

alloy was passive and the current during rubbing increased significantly due to mechanical depassivation.

3. At OCP the electrochemical response to rubbing could be modelled considering two limiting cases: galvanic coupling between wear track and surrounding surface and galvanic coupling between depassivated and still passive areas within the wear track.
4. In $NaNO_3$ the cathodic shift of the OCP is independent on load and of time. This indicates that galvanic coupling occurs within the wear track.
5. In NaCl solution the evolution of OCP with time, load and alloy hardness could be explained by the establishment of a galvanic coupling between wear track and surrounding surface. Quantitative predictions of the model were found to reasonably agree with experimental evidences.

Acknowledgments

The research team was financially supported by the Portuguese Foundation for Science and Technology (FCT–Portugal), under a PhD scholarship (SFRH/BD/27911/2006). The authors thank also to Dr.ª Edith Ariza (University of Minho) and Pierre Mettraux (EPFL) for SEM analysis.

Bibliography

[1] R.X. Li, R.D. Li, Y.H. Zhao, L.Z. He, C.X. Li, H.R. Guan, Z.Q. Hu, Age-hardening behavior of cast Al–Si base alloy, Materials Letters 58 (2004) 2096–2101.

[2] A.E. Jimenez, M.D. Bermudez, F.J. Carrion, G. Martınez-Nicolas, Room temperature ionic liquids as lubricant additives in steel–aluminium contacts: Influence of sliding velocity, normal load and temperature, Wear 261 (2006) 347–359.

[3] J. Qu, P.J. Blau, S. Dai, H. Luo, H.M. Meyer III, J.J. Truhan, Tribological characteristics of aluminium alloys sliding against steel lubricated by ammonium and imidazolium ionic liquids, Wear 267 (2009) 1226–1231.

[4] J. R. Davis, Aluminum and aluminum alloys, Edited by ASM International Handbook Committee, 1994, p.626-635.

[5] G. Wang, Q. Sun, L. Feng, L. Hui, C. Jing, Influence of Cu content on ageing behavior of AlSiMgCu cast alloys, Materials and Design 28 (2007) 1001–1005.

[6] H. Mindivan, M. Baydogan, E. S. Kayali, H. Cimenoglu, Wear behaviour of 7039 aluminum alloy, Materials Characterization 54 (2005) 263– 269.

[7] W.B. Bouaeshi, D.Y. Li, Effects of Y_2O_3 addition on microstructure, mechanical properties, electrochemical behaviour, and resistance to corrosive wear of aluminium, Tribology International 40 (2007) 188–199.

[8] J. Li, M. Elmadagli, V.Y. Gertsman, J. Lo, A.T. Alpas, FIB and TEM characterization of subsurfaces of an Al–Si alloy (A390) subjected to sliding wear, Materials Science and Engineering A 421 (2006) 317–327.

[9] D.P. Mondal, S. Das, R.N. Rao, M. Singh, Effect of SiC addition and running-in-wear on the sliding wear behaviour of Al–Zn–Mg aluminium alloy, Materials Science and Engineering A 402 (2005) 307–319.

[10] B. Venkataraman, G. Sundararajan, Correlation between the characteristics of the mechanically mixed layer and wear behaviour of aluminium, Al-7075 alloy and Al-MMCs, Wear 245 (2000) 22–38.

[11] S. Michler, Triboelectrochemical techniques and interpretation methods in tribocorrosion: A comparative evaluation, Tribology International 41 (2008) 573–583.

[12] I. Garcıa, D. Drees, J.P. Celis, Corrosion-wear of passivating materials in sliding contacts based on a concept of active wear track area, Wear 249 (2001) 452–460.

[13] S. Mischler, A. Spiegel, D. Landolt, The role of passive oxide films on the degradation of steel in tribocorrosion systems, Wear 225–229 (1999) 1078–1087.

[14] J. Perret, E. Boehm-Courjault, M. Cantoni, S. Mischler, A. Beaudouin, W. Chitty, J.-P. Vernot, EBSD, SEM and FIB characterisation of subsurface deformation during tribocorrosion of stainless steel in sulphuric acid, Wear 269 (2010) 383–393.

[15] ASTM G40-10b - Standard terminology relating to wear and erosion.

[16] C.N. Panagopoulos, E.P. Georgiou, A.G. Gavras, Corrosion and wear of 6082 aluminium alloy, Tribology International 42 (2009) 886–889.

[17] D. Landolt, S. Mischler, M. Stemp, Electrochemical Methods in tribocorrosion: a critical appraisal. Electrochimica Acta 46 (2001) 3913-3929.

[18] D. Landolt, Corrosion and Surfaces Chemistry of Metals, 1st ed., EPFL Press, 2007.

[19] N. Diomidis, J.-P. Celis, P. Ponthiaux, F. Wenger, Tribocorrosion of stainless steel in sulfuric acid: Identification of corrosion–wear components and effect of contact area, Wear 269 (2010) 93–103.

[20] H. Krawiec, V. Vignal, O. Heintz, P. Ponthiaux, F. Wenger, Local electrochemical Studies and Surface Analysis on Worn Surfaces, Journal of The Electrochemical Society 155 (2008).

[21] A.C. Vieira, A.M. Pinto, L.A. Rocha, S. Mischler, Effect of Al_2Cu precipitates size and mass transport on the polarization behaviour of age-hardened Al-Si-Cu-Mg alloys in 0.05 M NaCl, submitted to Electrochemica Acta.

[22] E. Sjölander, S. Seifeddine, The heat treatment of Al–Si–Cu–Mg casting alloys – Review, Journal of Materials Processing Technology 210 (2010) 1249–1259.

[23] J. Stojadinovic, D. Bouvet, M. Declercq, S. Mischler, Effect of electrode potential on the tribocorrosion of tungsten, Tribology International 42 (2009) 575–583.

[24] T. Ramgopal and G.S. Frankel, Role of Alloying Additions on the Dissolution Kinetics of Aluminum Binary Alloys Using Artificial Crevice electrodes, Corrosion 57 (2001) 702-711.

[25] I.M. Hutchings, Tribology: friction and wear of engineering materials, in: Metallurgy & Materials Science Series, Butterworth-Heinemann Publications, 2001.

[26] A.C. Vieira, A.R. Ribeiro, L.A. Rocha, J.P. Celis, Influence of pH and corrosion inhibitors on the tribocorrosion of titanium in artificial saliva, Wear 261 (2006) 994–1001.

[27] M. Pourbaix, Atlas of electrochemical equilibria in aqueous solutions, 2nd ed., National Ass. of corrosion engineers, 1974, p.168-175.

[28] P. Ponthiaux, F. Wenger, D. Drees, J.P. Celis, Electrochemical techniques for studying tribocorrosion processes, Wear 256 (2004) 459–468.

[29] K.-H. Z. Gahr, Microstructure and wear of materials, Tribology series 10 - Elsevier 1987.

[30] M. Stemp, S. Mischler, D. Landolt, The effect of mechanical and electrochemical parameters on the tribocorrosion rate of stainless steel in sulphuric acid, Wear 255 (2003) 466–475.

[31] H.J. Pearson, G.T. Burstein, R.C. Newman, Resistance of flow of current to starched electrodes, J. Electrochem. Soc.: Electrochemical Science and Technology 128, nº 11 (1981) 2297-2303.

[32] P. Jemmely, S. Mischler, D. Landolt, Electrochemical modeling of passivation phenomena in tribocorrosion, Wear 237 (2000) 63–76.

[33] M. Stemp, S. Mischler, D. Landolt, Electrochemical aspects of tribocorrosion, Tribology and Interface Engineering Series 39 (2001) 539-547.

[34] M. Stemp, Doctoral Thesis EPFL, No. 2292, (2001).'Tribocorrosion mechanisms of passivating metals under sliding wear conditions'

[35] Modern aspects of Electrochemistry, Springer, Vol. 44, p.465-468.

[36] M. Schütze, Materials Science & Technology, Vol.1, Corrosion and Environment (2000), 285-382.

[37] Modern aspects of Electrochemistry, Plenum Press, Vol. 23, p.159-167.

[38] H Kaesche, Corrosion of Metals, Springer (2003), p.308.

List of Figures:

Figure 11: Chemical and mechanical wear contribution on the total wear volume obtained for all the samples after the tribocorrosion tests in 0.1M $NaNO_3$ under anodic applied potential (Conditions: 4N).

Figure 12: Simulation of the cathode potential E_c evolution during rubbing for i_a = 9.5 mA/cm^2.
The experimental data were selected from Figure 8a).

Figure 13: Simulation for i_a = 9.5 mA/cm^2 of the potential evolution in the anode and in the cathode areas during a tribocorrosion experiment. The ohmic resistance was calculated according to [31] taking into account the evolution of the wear track width during rubbing.

List of Tables:

Table 1

		0.05M NaCl		0.1M $NaNO_3$	
Load	**Samples**	**Outside***	**Inside ****	**Outside ***	**Inside ****
4N	*Al-NHT*	80 ± 3	101 ± 17	77 ± 4	108 ± 12
	Al-S2h	115 ± 6	146 ± 3	94 ± 5	137 ± 20
	Al-S8h	111 ± 5	142 ± 17	115 ± 4	154 ± 19
1.3N	*Al-NHT*	69 ± 8	117 ± 23	80 ± 3	101 ± 14
	Al-S2h	81 ± 11	123 ± 26	115 ± 4	144 ± 16
	Al-S8h	120 ± 12	140 ± 16	114 ± 11	157 ± 38

* Outside – Measurements made outside of the wear track; ** Inside – Measurements made inside of the wear track

Figure

Figure 1

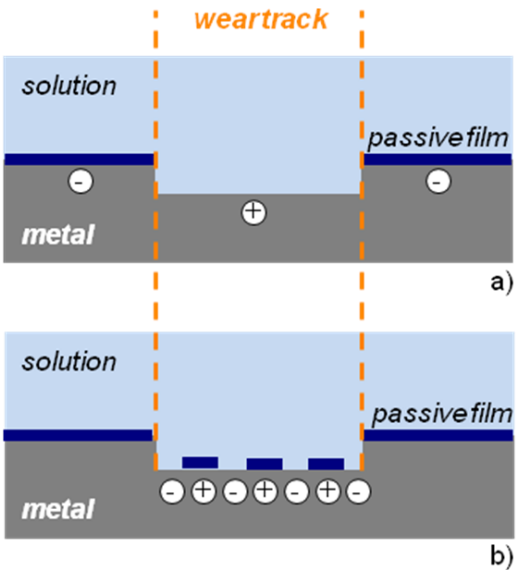

Figure 2

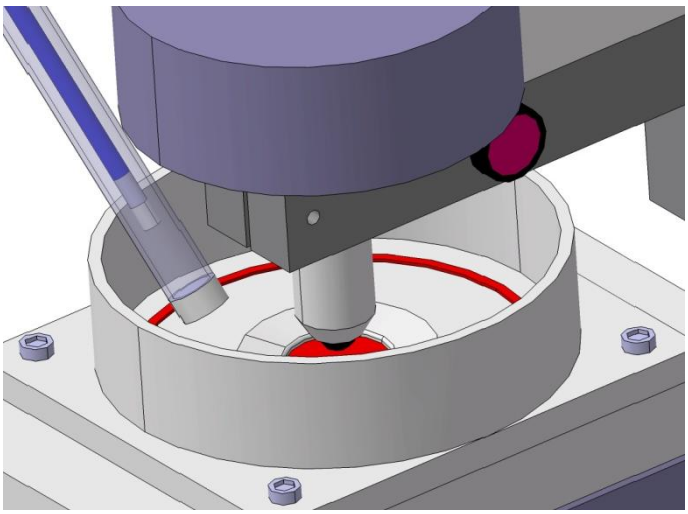

Figure 3

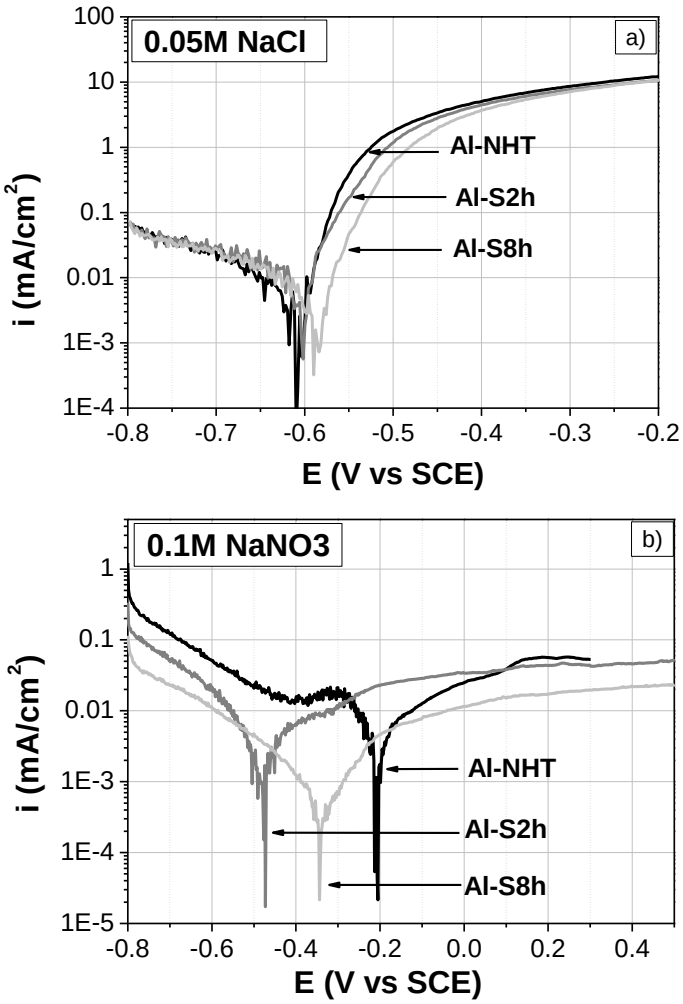
0.05M NaCl
a)
Al-NHT
Al-S2h
Al-S8h
i (mA/cm²)
E (V vs SCE)
0.1M NaNO3
b)
Al-NHT
Al-S2h
Al-S8h
i (mA/cm²)
E (V vs SCE)

Figure 4

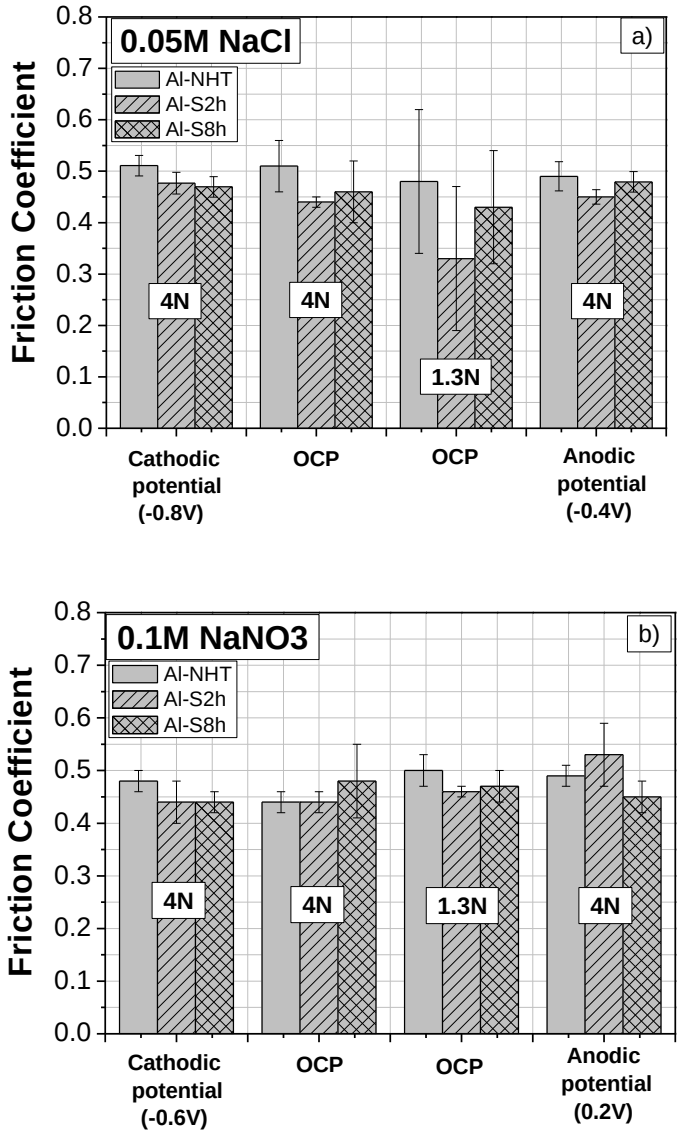
0.05M NaCl
a)
Al-NHT
Al-S2h
Al-S8h
Friction Coefficient
0.0
0.1
0.2
0.3
0.4
0.5
0.6
0.7
0.8
4N
4N
1.3N
4N
Cathodic potential (-0.8V)
OCP
OCP
Anodic potential (-0.4V)
0.1M NaNO3
b)
Al-NHT
Al-S2h
Al-S8h
Friction Coefficient
4N
4N
1.3N
4N
Cathodic potential (-0.6V)
OCP
OCP
Anodic potential (0.2V)

Figure 5

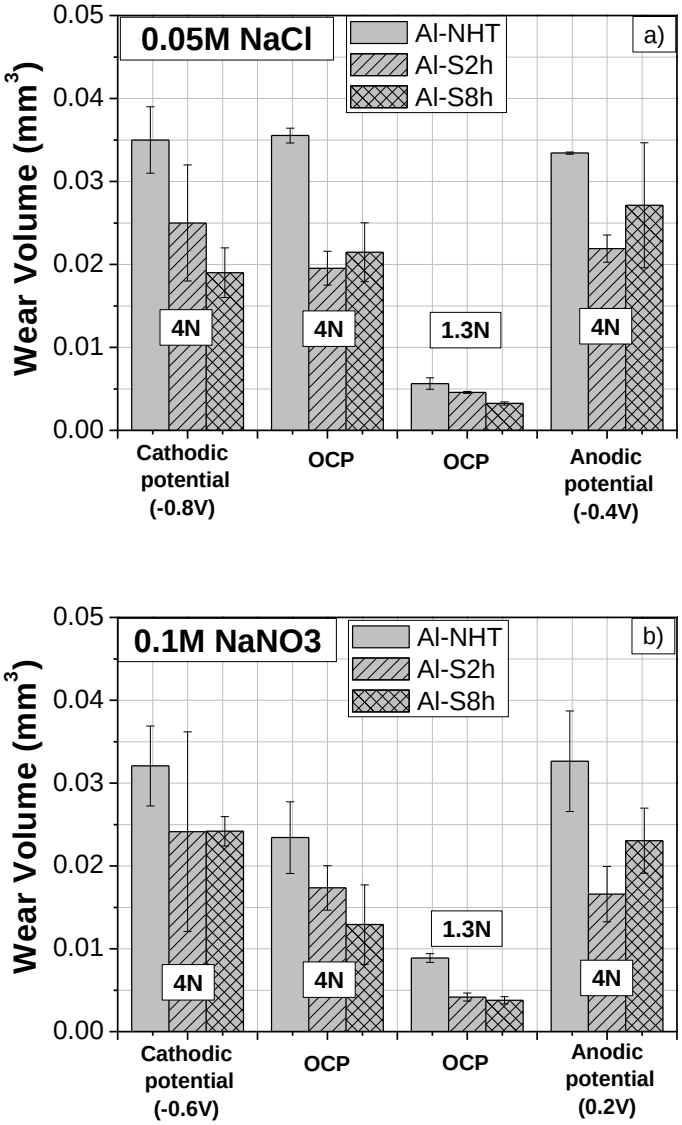
0.05M NaCl
Al-NHT
Al-S2h
Al-S8h
a)
Wear Volume (mm3)
0.05
0.04
0.03
0.02
0.01
0.00
4N
4N
1.3N
4N
Cathodic potential (-0.8V)
OCP
OCP
Anodic potential (-0.4V)
0.1M NaNO3
Al-NHT
Al-S2h
Al-S8h
b)
Wear Volume (mm3)
0.05
0.04
0.03
0.02
0.01
0.00
4N
4N
1.3N
4N
Cathodic potential (-0.6V)
OCP
OCP
Anodic potential (0.2V)

Figure 6

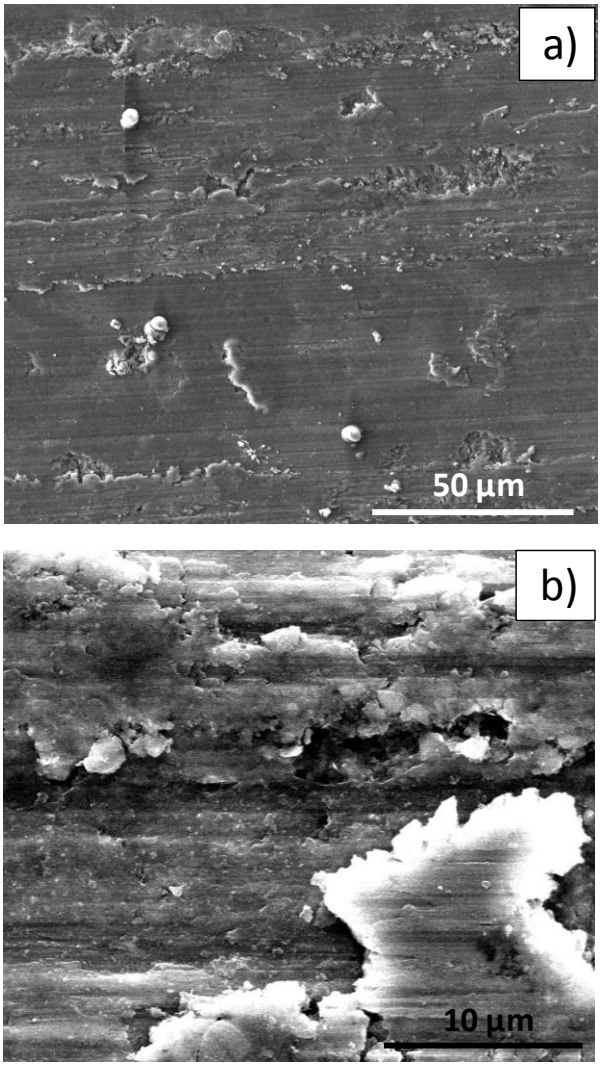

Figure 7

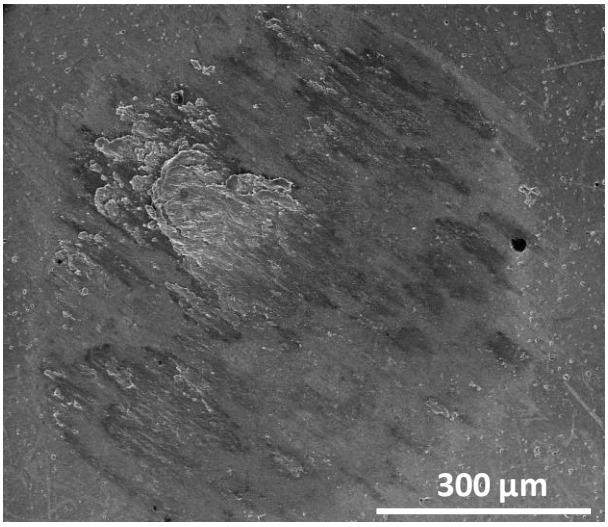

Figure 8

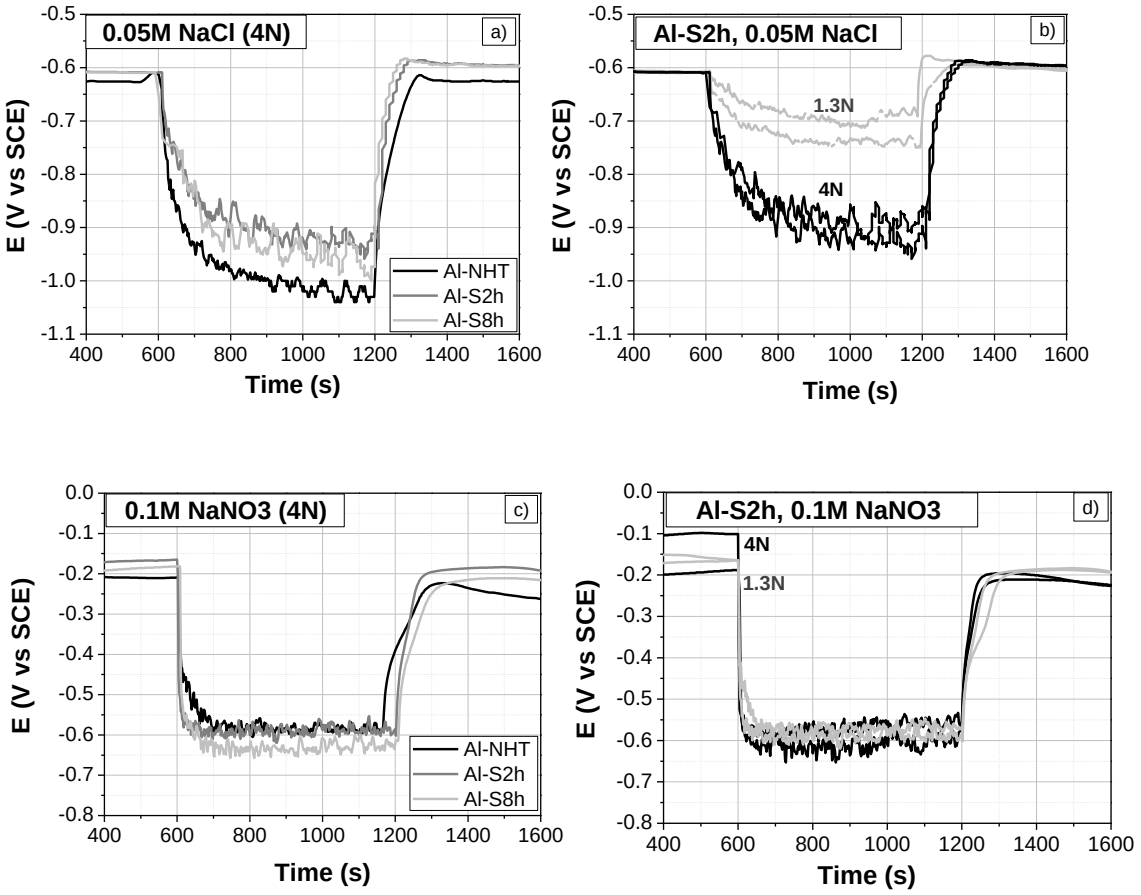
0.05M NaCl (4N)
a)
Al-NHT
Al-S2h
Al-S8h
E (V vs SCE)
Time (s)
Al-S2h, 0.05M NaCl
b)
1.3N
4N
E (V vs SCE)
Time (s)
0.1M NaNO3 (4N)
c)
Al-NHT
Al-S2h
Al-S8h
E (V vs SCE)
Time (s)
Al-S2h, 0.1M NaNO3
d)
4N
1.3N
E (V vs SCE)
Time (s)

Figure 9

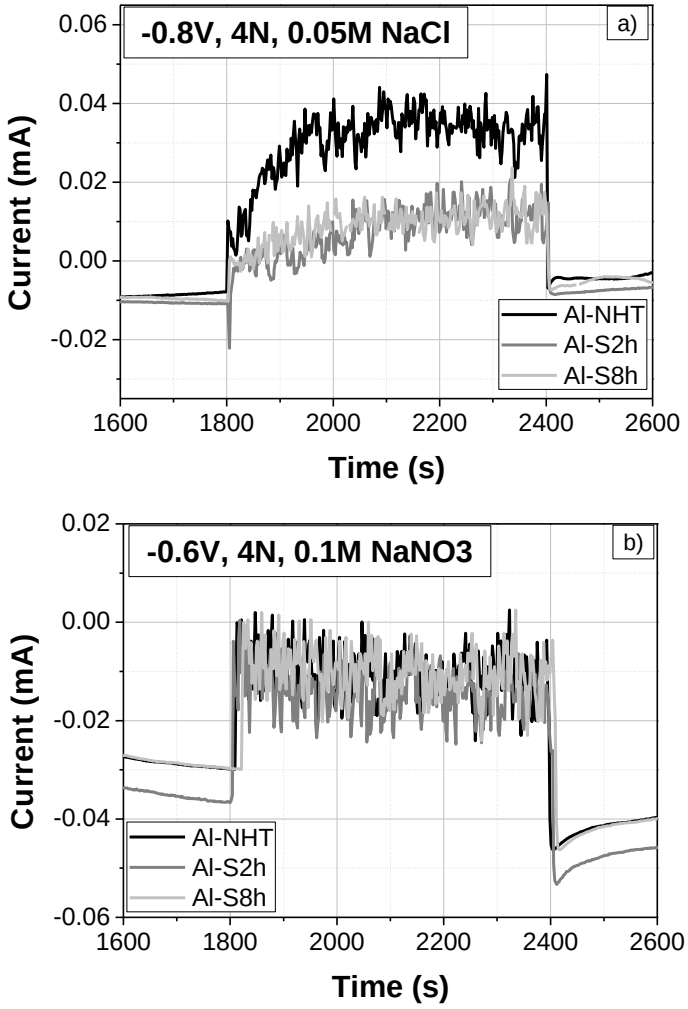
-0.8V, 4N, 0.05M NaCl
a)
Current (mA)
Time (s)
Al-NHT
Al-S2h
Al-S8h
-0.6V, 4N, 0.1M NaNO3
b)
Current (mA)
Time (s)
Al-NHT
Al-S2h
Al-S8h

Figure 10

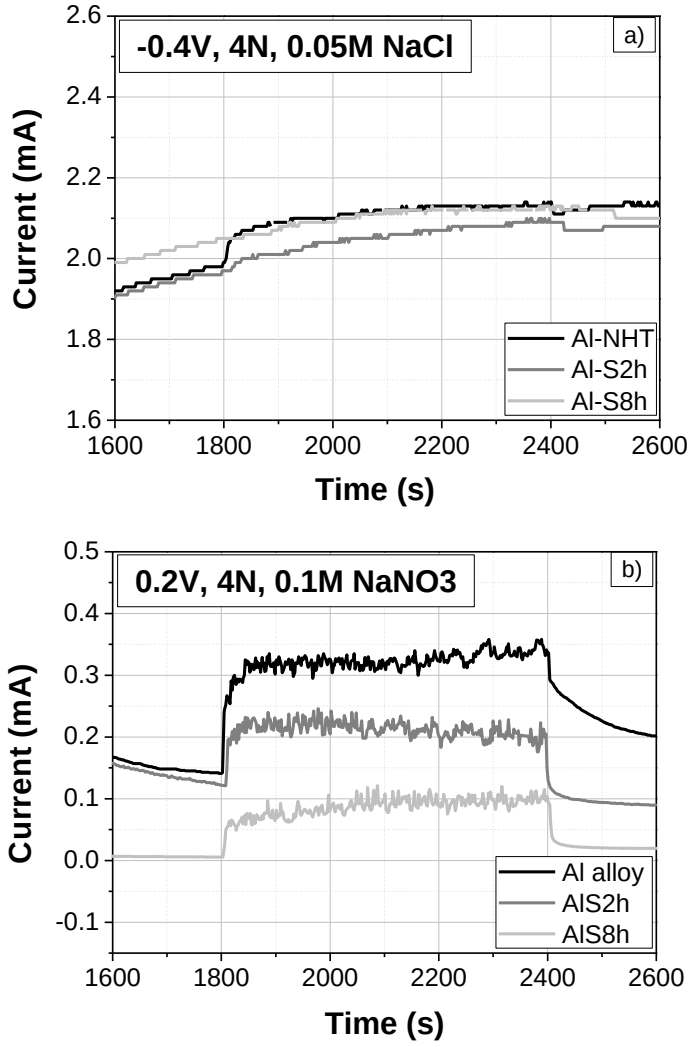
-0.4V, 4N, 0.05M NaCl
a)
Current (mA)
Time (s)
Al-NHT
Al-S2h
Al-S8h
0.2V, 4N, 0.1M NaNO3
b)
Current (mA)
Time (s)
Al alloy
AlS2h
AlS8h

Figure 11

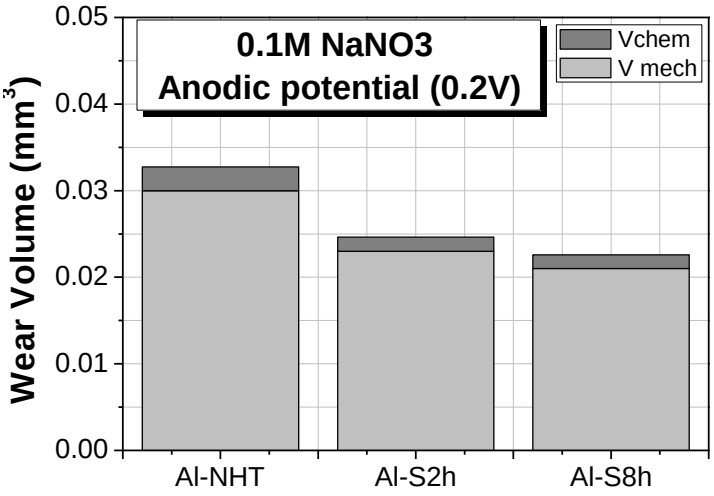
0.1M NaNO3
Anodic potential (0.2V)
Vchem
V mech
Wear Volume (mm3)
0.05
0.04
0.03
0.02
0.01
0.00
Al-NHT
Al-S2h
Al-S8h

Figure 12

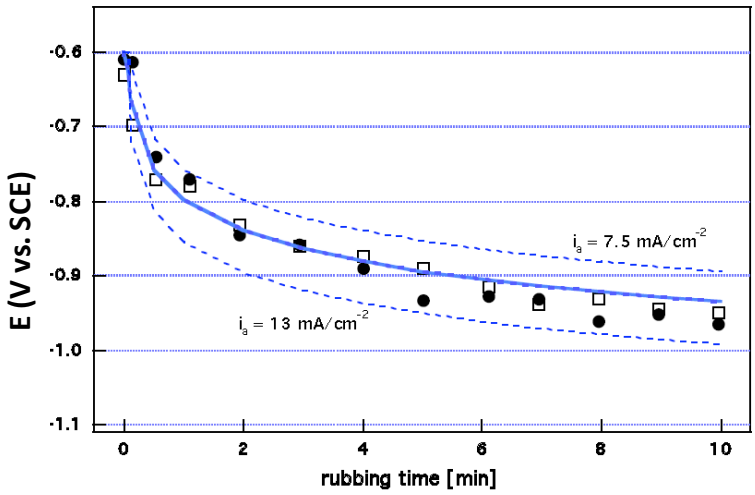
-0.6
-0.7
-0.8
-0.9
-1.0
-1.1
E (V vs. SCE)
0
2
4
6
8
10
rubbing time [min]
i_a = 7.5 mA/cm^{-2}
i_a = 13 mA/cm^{-2}

Figure 13

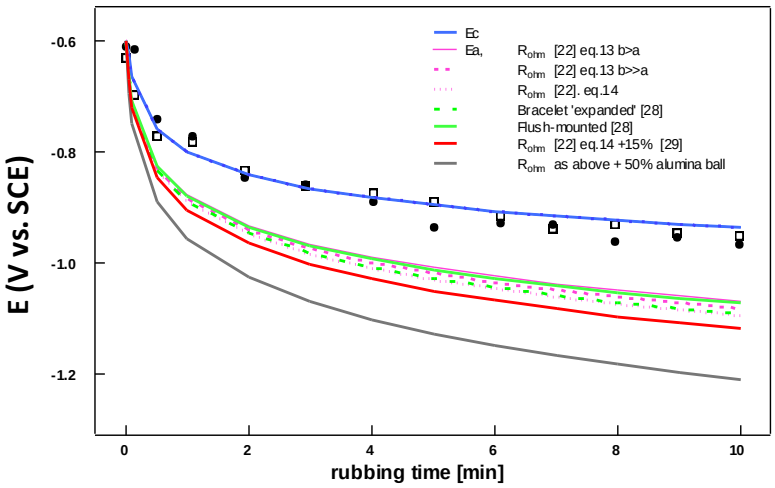
Ec
Ea,
$R_{o/m}$ [22] eq.13 b>a
$R_{o/m}$ [22] eq.13 b>>a
$R_{o/m}$ [22]. eq.14
Bracelet 'expanded' [28]
Flush-mounted [28]
$R_{o/m}$ [22] eq.14 +15% [29]
$R_{o/m}$ as above + 50% alumina ball
E (V vs. SCE)
-0.6
-0.8
-1.0
-1.2
0
2
4
6
8
10
rubbing time [min]